galaxies

MDPI

Article

A Scattered Star Group in the Orion A Region of the Milky Way

Sergei Vereshchagin [1,*,†], Natalya Chupina [1,†], Kristina Lyzenko [1,2], Anatoly Kalinkin [1,3], Nikolay Kondratev [1,2], Dana Kovaleva [1,†] and Sergei Sapozhnikov [1]

[1] Institute of Astronomy of the Russian Academy of Sciences, 119017 Moscow, Russia; chupina@inasan.ru (N.C.); kristy-002@yandex.ru (K.L.); kalinkintolya@yandex.ru (A.K.); rjkz2792009@rambler.ru (N.K.); dana@inasan.ru (D.K.); thestriks@gmail.com (S.S.)
[2] Department of Astrophysics and Stellar Astronomy, Physics Faculty, Lomonosov Moscow State University, 119991 Moscow, Russia
[3] Department of Experimental Astronomy, Physics Faculty, Lomonosov Moscow State University, 119991 Moscow, Russia
* Correspondence: svvs@ya.ru
† These authors contributed equally to this work.

Abstract: Using Gaia DR3 data, we identified an extended a ∼60 pc group of stars sharing common motion but scattered in space, including from 150 to 300 probable members, named Group V. It can be associated with a group identified by Getman et al. (2019) and by Jerabkova et al. (2019) as a relic of a gas filament, traced by the mutual position of stars after the gas is swept out. We estimate its age to be approximately 16 million years. A combination of methods is applied to select probable members of Group V. We discuss the kinematic characteristics of the stars of Group V and the controversial clues they provide for understanding its nature. Due to the vicinity of a number of open clusters in the space, differentiating between members of the group and of the clusters is problematic, and mutual contamination is inevitable. The pair of clusters Gulliver 6 and UBC 17b is wrapped inside Group V but differs from it in kinematics.

Keywords: star clusters; space missions; Gaia; Milky Way; Orion A

Citation: Vereshchagin, S.; Chupina, N.; Lyzenko, K.; Kalinkin, A.; Kondratev, N.; Kovaleva, D.; Sapozhnikov, S. A Scattered Star Group in the Orion A Region of the Milky Way. *Galaxies* **2023**, *11*, 99. https://doi.org/10.3390/galaxies11050099

Academic Editors: Vladimir Korchagin, Orchidea Maria Lecian and Maxim Yu. Khlopov

Received: 15 August 2023
Revised: 11 September 2023
Accepted: 15 September 2023
Published: 19 September 2023

1. Introduction

In general, in the vicinity of the Orion A molecular cloud, which is one of the most actively researched areas in the Galaxy, a stellar-gas complex is presented before our eyes, in which evidence of many physical processes is observed, including the formation of open star clusters (OSC), the decay of OSCs, and a supernova explosion, a possible result of the collision of two molecular clouds.

The Gaia space mission [1] has provided highly accurate data on the positions and velocities of more than 1.5 billion stars in three-dimensional space, allowing us to revolutionize many of our ideas about the structure and populations of our Galaxy. Thus, the combination of Gaia astrometric and photometric data has been widely used to isolate probable members of OSCs with previously unattainable accuracy and to detect previously unknown star clusters, since the publication of the second release of Gaia data, DR2 [2]; see, e.g., Castro-Ginard et al. [3,4,5], Cantat-Gaudin et al. [6], Cantat-Gaudin and Anders [7].

In addition, the high accuracy of Gaia data makes it possible to separate extended low-density stellar structures from the background in the multidimensional data space, the detection and investigation of which was previously significantly difficult. These structures—moving stellar groups and streams representing the remnants of dissolved open star clusters and associations, tidal tails of OSC, and their crowns formed when the cluster lost mass at an early stage of its evolution—are actively detected and investigated (see, for example, [8–12]).

As part of the third data release (DR3), Gaia updated its astrometric and photometric data [13] combined with, among other things, radial velocities for more than 33 million

stars [14]. This motivated the authors to turn to the study of an intriguing area in Orion A, including the Orion Sword OSCs chain and the surrounding stellar background, which includes a complex of young stellar aggregates [15]. In front of Orion cloud A, there is a rich stellar population comprising B to M stars. Calculations of spatial movements of gas clouds Orion A and Orion B showed that they were located near each other about 6 million years ago, and now they are moving away radially from approximately the same region of space [16]. The spatial distribution of this population peaks around NGC 1980. It is concluded that the age of NGC 1980 is about 4–5 Myr, with an estimated population at about 2000 stars. This makes NGC 1980 one of the most massive clusters in the entire Orion complex [17]. Within 1.5° around the Orion Nebula Cluster (ONC), several adjacent and probably overlapping open star clusters (OSC) and groups of young stars (young stellar objects, YSO) are observed. The latter include the well-known grouping of young stars σ Orionis, studied in detail in [18]. In the course of the investigation of the σ Orionis region, they found an increase in the density of stars in phase space that is not associated with any of the previously known star clusters in the adjacent region of space. This study is devoted to the investigation of the characteristics and nature of the detected object. In [18], a study of the three-dimensional structure, kinematics, and age distribution of the Orion association based on Gaia DR2 data was published. In [16], an expansion of the studied clouds on a scale of 100 pc was detected, which implies a history of star formation based on feedback, probably from previous generations of massive stars.

The paper is organized as follows. In Section 2, we discuss the allocation of the probable members of the discovered group of stars. Section 3 is dedicated to the resulting characteristics of the detected structure. A discussion of its probable origin, evolution, and interaction with surrounding objects in the field of star formation is presented in Section 4. Section 5 contains the conclusions we have proposed.

2. Materials and Methods

While analyzing the proper motion (PM) diagram $\mu_\alpha - \mu_\delta$ of a sample of stars in the region of a group of young stars σ Orionis [18] with Gaia DR3 data [13,14], an increase in the density of stars was visually detected in the area of the diagram not associated with the proper motions of σ Orionis. Figure 1 (bottom-left panel) represents the proper motion diagram (PMD), which attracted our attention, and the position of the discussed group is marked with a red circle. At the same time, both on the diagram of its own movements and in space, the specified group seems to be sparse. For convenience, hereafter, we will name it Group V.

Stellar groups in the discussed region are quite complex and tangled for a number of reasons. This includes their close vicinity and similar origin and the presence of embedded structures. Last but not least, the position of the Ori complex with respect to the observer in the Galaxy makes absolute values of the typical proper motions of stars in this region close to zero, which results in an increase in its relative errors. To handle these difficulties, we apply several different methods to select probable members of Group V and then combine the results.

2.1. Direct Approach

We selected from Gaia DR3 all the sources from the circle centered at ($\alpha = 84.0°$, $\delta = -5.3°$) of a radius $R = 5°$ that satisfy the condition on parallax: 2.2 mas $< \varpi <$ 3 mas. This list included 38,474 sources.

Figure 1 (bottom-right panel) represents these sources on the PMD, and Figure 1 (top panel) represents the sources on the α–δ. In both figures, we mark the location of known open clusters. They are multiple and overlap at the projection (Figure 1, top panel); however, in Figure 1 (bottom-right panel), one may see that the probable location of Group V (marked in red) is well separated from the concentrations of sources identified as probable members of the open clusters.

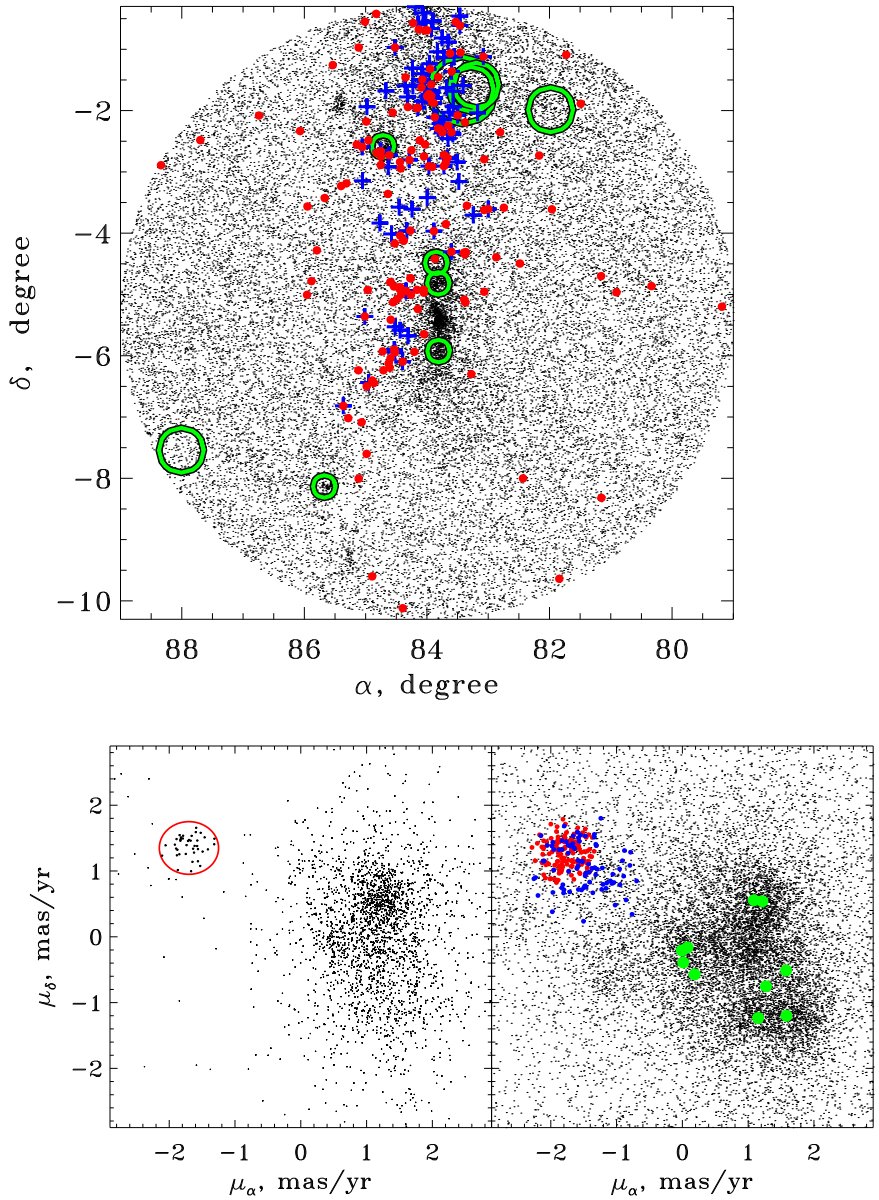

Figure 1. (**Top panel**): The position of the stars of our sample in the equatorial coordinate system. The red dots represent the stars of Dataset A. The blue crosses show the stars of the Dataset B. The green circles mark the positions of the open clusters ASCC 19, Gulliver 6, L 1641S, NGC 1977, NGC 1980, Sigma Ori, UBC 17a, UBC 17b, UBC 207, and UPK 422. The sizes of the circles are proportional to the radii of the clusters. (**Bottom-left panel**): PMD that singles out Group V. (**Bottom-right panel**): The PMD for stars located in the Orion region. The red dots represent the stars of Dataset A. The blue dots show the stars of Dataset B. The green filled circles mark the proper motion of the clusters in the region under consideration (ASCC 19, Gulliver 6, L 1641S, NGC 1977, NGC 1980, Sigma Ori, UBC 17a, UBC 17b, UBC 207, and UPK 422).

Stars are selected as candidates for members of Group V if their proper motions satisfy the condition based on initial discovery (Figure 1, bottom-left panel): for proper motions, the area is limited by a circle with a radius of 0.5 mas/yr and centered at $\mu_\alpha = -1.8$ mas/yr, $\mu_\delta = 1.3$ mas/yr. Thus, 330 sources were initially selected. After checking their distribution in the diagram $G_{mag} - \varpi$ (Figure 2), we find that initial selection includes a structure at about $\varpi \approx 2.4$ mas, as well as a significant fraction of contaminating sources. To refine our dataset, we apply an iterative procedure calculating the mean parallax $\bar{\varpi} \pm \sigma_\varpi$ and discarding sources out of σ_ϖ. This procedure results in data selection including 150 stars

with parallaxes in mas in the range of $2.32 \leq \varpi \leq 2.50$ with a mean value $\bar{\varpi} = 2.41$ mas. We use this dataset for reference, and for convenience hereafter, we will name it Dataset A (see Table A1 in Appendix A). In Figure 1 (top panel), the stars of Dataset A are marked with red dots. They are sparsely distributed, featuring a long concentration extending over some six degrees.

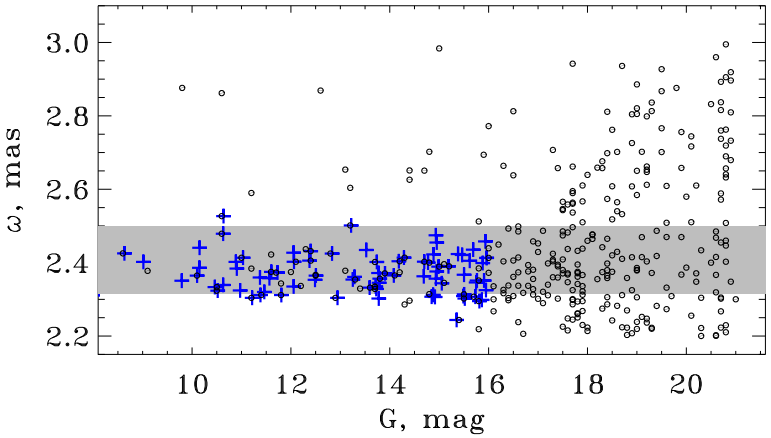

Figure 2. Parallax-magnitude diagram for the stars of our initial sample (black dots, $n = 330$). The blue crosses show the stars of Dataset B. The gray strip in parallaxes 2.32 mas $\leq \varpi \leq$ 2.50 mas is limiting the Dataset A.

2.2. Statistical Method

Due to the discovered extent of Group V, we further apply the method of selection of its probable members that does not focus on the agreement of the proper motions but on the spatial velocities of the sources. Dataset A contains 38 sources with radial velocities in Gaia DR3. Their distribution has a peak and a median value at $RV_0 = 26.5$ km/s. We use this estimate and proper motion to obtain the expected spatial velocity of the members of Group V.

The respective space velocities are obtained as

$$\begin{bmatrix} U \\ V \\ W \end{bmatrix} = V_r \cdot \begin{bmatrix} \cos l \cos b \\ \sin l \cos b \\ \sin b \end{bmatrix} + \frac{\kappa \mu_l}{\varpi} \cdot \begin{bmatrix} -\sin l \\ \cos l \\ 0 \end{bmatrix} + \frac{\kappa \mu_b}{\varpi} \cdot \begin{bmatrix} -\cos l \sin b \\ -\sin l \sin b \\ \cos b \end{bmatrix} \quad (1)$$

where $\kappa = 4.74047$ is the transformation factor from 1 mas/yr at 1 kpc to 1 km/s, and the mean values for coordinates, parallaxes, and proper motions are obtained based on Dataset A.

We use a modification of the convergent point method described by [19] to calculate for each source the kinematic probability of its relation to Group V similarly to the idea described in [20]. The kinematic probability $P^k_{\rm kin}$ for a $k^{\rm th}$ star to belong to the investigated system is defined as

$$P^k_{\rm kin} = \exp\left\{ -\frac{1}{4} \left[\left(\frac{\mu^k_l - \mu^k_{l_{exp}}}{\varepsilon_{\mu_l}} \right)^2 + \left(\frac{\mu^k_b - \mu^k_{b_{exp}}}{\varepsilon_{\mu_b}} \right)^2 \right] \right\}, \quad (2)$$

where

$$\mu^k_{l_{exp}} = (-\sin l_k \cdot U + \cos l_k \cdot V) / (\kappa / \varpi_k);$$
$$\mu^k_{b_{exp}} = (-\cos l_k \sin b_k \cdot U - \sin l_k \sin b_k \cdot V + \cos b_k \cdot W) / (\kappa / \varpi_k)$$

are values of proper motion in (l, b) for a given coordinates l_k, b_k, and ϖ_k expected for the stars sharing space motion (U, V, W) of Group V. Scattering parameters of the proper motion $\varepsilon_{\mu_l}, \varepsilon_{\mu_b}$ were set to 1.0 mas/yr.

We also use the estimate of the age of Group V obtained with Dataset A ($\log t \approx 7.2$; see discussion in Section 3) to calculate the photometric probabilities to be coeval to the group for all the sources of investigated region. Photometric probabilities $P^k_{\rm ph}$ are calculated similarly to [20].

We suggest that the Group V abundance is close to the solar one, based on the abundances of nearby clusters UBC 17b and Gulliver 6. Recent investigation with GALAH [21] provides $[Fe/H] = -0.098 \pm 0.058, -0.070 \pm 0.032$ for them, respectively. Isochrones based on the calculations by [22] for solar metallicity were obtained from the Padova webserver CMD3.3 [1].

Photometric probability $P^k_{\rm ph}$ is computed in CMD $G, BP - RP$ as follows. It is set equal to 1 for the stars occupying in CMD an area in between the isochrones for single stars and for unresolved binaries of equal mass. For all the other stars, the photometric probability depends on a difference between magnitudes

$$\Delta G^i = \min\Big(|G^i - G^b|, |G^i - G^f|\Big) \tag{3}$$

where G^b, G^f are brighter and fainter values of magnitude, respectively, limiting the domain between the isochrones for single stars and for unresolved binaries of equal mass for a given color $BP - RP$:

$$P^k_{\rm ph} = \exp\left\{-\frac{1}{2}\left(\frac{\Delta G^k}{\varepsilon^k_G}\right)^2\right\}. \tag{4}$$

The value of ε^k_G is defined by individual parallax error σ^k_ϖ/ϖ and photometric error σ^k_G of the kth star.

The resulting probability is obtained, also according to [20], as

$$P^k_{tot} = \min(P^k_{\rm kin}, P^k_{\rm ph}), \tag{5}$$

and the kth star is considered to be a probable member of Group V if $P^k_{tot} \geq 0.6$. We find 344 sources satisfying this condition which are presented in Figure 3.

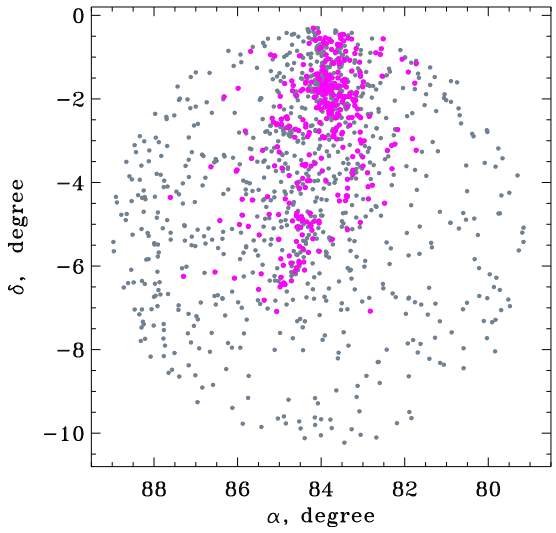

Figure 3. The result of the selection of probable members of Group V via the statistical method. Grey dots—all stars; magenta dots—stars with a membership probability $P_{tot} > 0.6$.

2.3. Application of Clustering Algorithm

Independently, we used the unsupervised clustering algorithm described in [23] to reveal the extended groups of stars sharing common motion. This includes the search for pairs of stars with a projected separation S_{proj} below an established maximum and a difference in tangential velocities ΔV_t less than an accepted value. After the catalog of such pairs is compiled, the DBSCAN algorithm [24] is applied to it. This scheme proved to be effective for spatially extended stellar structures. In the present case, the limiting value for the projected distance between the components of a pair was set to $S_{proj} < 5$ pc, and the difference in tangential velocities was selected as $V_t < 1$ km/s. These limits are quite strict, which is motivated by the complicated nature of the Orion region and numerous prospective sources of contamination. As a result, two clusters of sources are selected (due to their spatial separation), as presented in Figure 4. The joint dataset selected with the clustering algorithm includes 737 sources. The clustering algorithm here helps to define the position of the group of stars in the spatial coordinates.

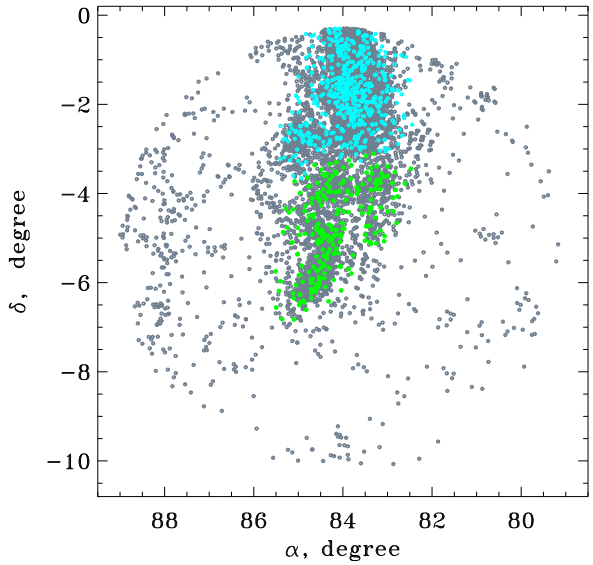

Figure 4. The result of the selection of probable members of Group V via the clustering algorithm applied to the compiled catalog of pairs. Grey dots—all pairs (medium position); green and cyan dots—selected clusters of stars.

The clustered sources in Figure 4 are divided into two groups due to the non-uniformity of their distribution in the space of coordinates. They are similar in all other respects, so we also join them.

2.4. The Resulting Dataset

Due to the similar ages of sources in Orion, the diversity of extinction across the region, etc., the dataset obtained with the statistical method is contaminated. One may state the same with respect to the dataset obtained with the clustering algorithm that met problems with the definition of limits of a cluster in dense surroundings and large relative errors with the calculation of difference in V_t. To decrease the effect, we, firstly join these two datasets to select only the stars that are included in both of them. This leaves us with 319 probable members. Secondly, we compare the distribution in space of all 319 of these sources with the distribution of the brighter of them ($G_{mag} < 16$). We find that in the RA, Dec plane, these distributions are similar. In parallax, however, both distributions have a pronounced maximum, but the distribution of all probable members also has extended and populated wings that lack the distribution of brighter members. This suggests that parallaxes are systematically less accurate for the stars fainter than $G_{mag} \approx 16$ and agrees with the notion on Gaia astrometry [25]. This is why we choose to use only the dataset of brighter stars

to investigate the spatial structure and kinematics of Group V. We select only stars with $G_{mag} < 16$, which are probable members of Group V, both based on statistical selection and based on the application of the clustering algorithm. There are 97 stars satisfying these conditions. We refine this dataset from outliers based on its distribution over the parallax with an iterative procedure to discard stars out of $3\sigma_{\varpi}$. The resulting, final dataset, hereafter named Dataset B (see Table A2 in Appendix A), contains 87 stars brighter than $G_{mag} = 16$. Remarkably, the distribution of these stars over parallaxes perfectly fits Dataset A (Figure 2) and follows its distribution in the RA, Dec plane (see Figure 1, top panel). In the proper motion diagram (Figure 1, bottom-right panel), Dataset B is more liberal than Dataset A, covering a wider span of proper motions due to different methods of selection.

Our main purpose is to reveal the bona fide members of Group V. This means we unavoidably miss a number of members. The extended scattered group V is unlike the star cluster, which has a relatively predictable form and extension, so it is difficult to estimate this number. However, the lower estimate may lay in the results of statistical selection (Section 2.2), which chooses only 1σ members comprising 68% of the full sample. Thus, we may expect that we miss at least the third part of the probable members of Group V.

3. Results

We used the isochrones obtained from the Padova webserver CMD3.3 [2] based on the calculations by [22] for solar metallicity $Z = 0.0152$, to estimate the age of Group V. Figure 5 (left panel) represents the color–magnitude diagram of the Dataset A, and Dataset B. To pass to de-reddened values, we used Gaia DR3 estimates of $A_G, E(BP - RP)$. They are available for 100 stars from Dataset A with $G_{mag} > 18$. The absolute magnitudes of the stars were calculated using Gaia parallaxes. Figure 5 (right panel) represents the resulting de-reddened diagram in absolute stellar magnitudes. The overlaid isochrones are for 1 Myr, 10 Myr, 16.8 Myr, and 100 Myr. The locations of the sources of Dataset A agree well with the age of about 16 Myr ($\log t \approx 7.2 \pm 0.3$).

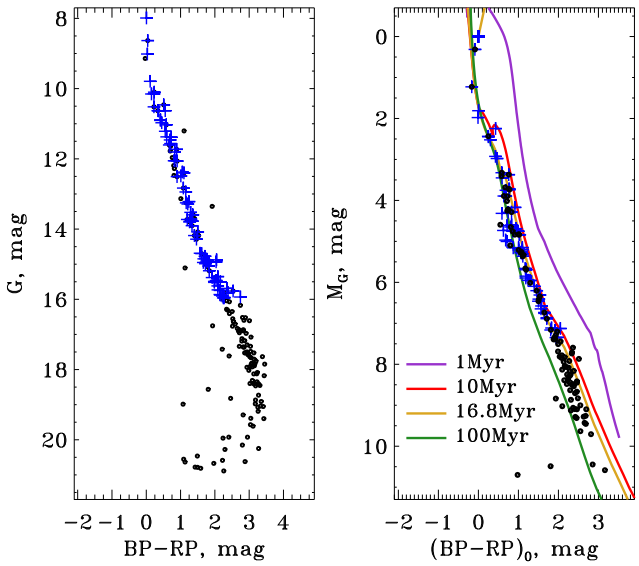

Figure 5. Color–magnitude diagram of Group V, observed (**left**), de-reddened (**right**). The black dots represent the stars of Dataset A. The blue crosses show stars of Dataset B. Isochrones were obtained from the Padova webserver CMD3.3 (see text).

In Table 1, we sum up the characteristics of Group V.

Table 1. Group V. General characteristics based on Datasets A, B *.

Parameter	Mean_A	Error_A	Mean_B	Error_B	Mean_B_0 ***	Units
$\bar{X}$	−351	1	−360	1	–	pc
D_X **	52	–	48	–	54	pc
$\bar{Y}$	−184	1	−178	1	–	pc
D_Y **	61	–	48	–	60	pc
$\bar{Z}$	−132	1	−129	1	–	pc
D_Z **	63	–	28	–	9	pc
U	21.6	2.5	24.9	1.8	–	km/s
V	−7.1	1.2	−8.7	0.9	–	km/s
W	−9.4	1.0	−10.2	0.6	–	km/s
N	150	–	83	–	–	–
Age	16	50%	16 ****	–	–	Myr

* Galactic coordinates and velocities are provided in the heliocentric system. ** D_X, D_Y, D_Z are $X_{max} - X_{min}$, $Y_{max} - Y_{min}$, $Z_{max} - Z_{min}$ for the dataset. *** 16 Myr ago, results obtained with backward orbit integration. See Section 4 for details. **** By definition, age is used for data selection.

Figure 6 shows the distribution of stars in Dataset A ($n = 150$) and in Dataset B ($n = 83$) in the Cartesian coordinate system. The distances of stars from the Sun, determined by the classical parallax formula, were used. The nearest OSCs located in this region of space are also shown. A rectangular galactic heliocentric coordinate system is used, in which the X axis is directed to the Galactic Center (l = 0°, b = 0°), the Y axis is in the direction of the Galaxy rotation (l = 90°, b = 0°), and the Z axis is directed to the North Pole of the Galaxy (b = 90°). The same coordinate system is used for spatial velocities.

Figure 7 shows the distribution of stars of Dataset A and Dataset B in the 2D plane, and the dimensions of each 2D region in terms of (D_X, D_Y, D_Z) are approximately (60, 60, 70) pc, respectively. The distribution of stars within the region is not uniform in density, although the region as a whole is approximately symmetrical in space.

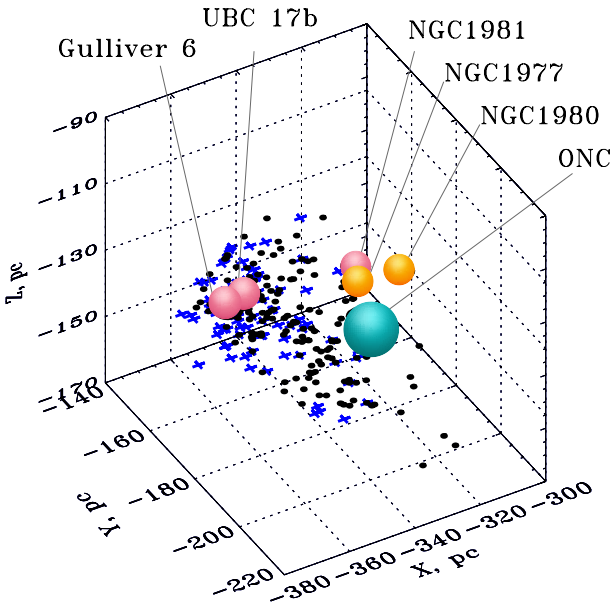

Figure 6. Three-dimensional distribution of the stars of Group V. Dataset A—black dots; Dataset B—sky blue crosses. The balls indicate the positions and approximate characteristic dimensions of the OSCs. The color of the balls indicates the age of the OSC: the age increases from blue to orange and to red. The ages of the clusters range from 1 million years (ONC) to 17 million years (Gulliver 6).

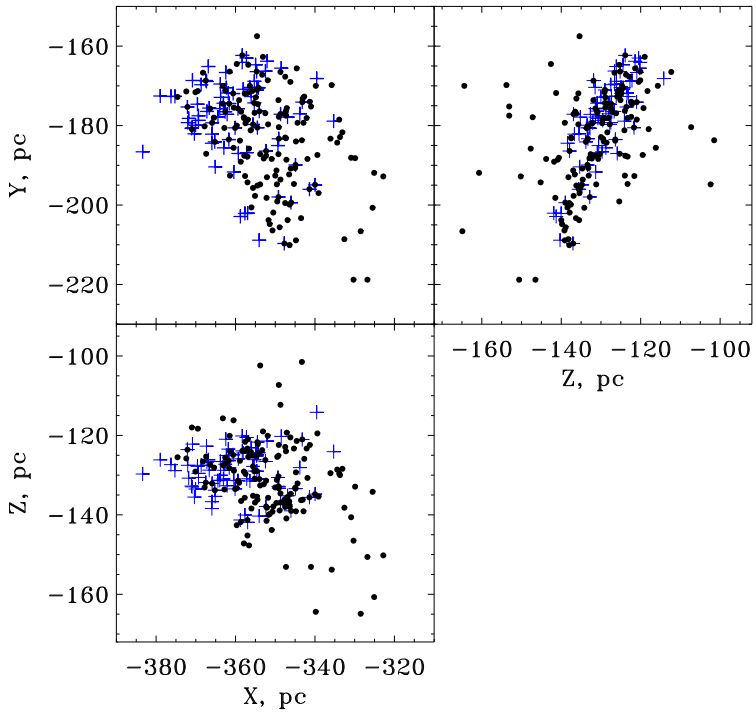

Figure 7. Positions of stars of group V. Dataset A—black dots; Dataset B—blue crosses.

4. Discussion

The fragmentation of giant gas clouds leads to the formation of stellar complexes and stellar associations, including hundreds of star clusters. Most of them decay in the first 10 million years [26]. A study by Getman et al. (2019) [27] showed the presence of many YSO stars in the Orion A region. Since their evolution time is on the order of a million years according to Peña and Morrell (2019) [28], the presence of YSO indicates an extremely young age of the group under study. Our group includes several YSOs, for example, Gaia DR3 ID 3016918241416381824, 3017010673409444992, and Gaia DR2 3017016475908135808. This testifies in favor of the young age of the considered group. YSOs are associated with phenomena of early stellar evolution: jets, masers, Herbig–Haro objects, and protoplanetary disks.

The discovered group is very young, and it may represent the remnants of a dissolving cluster or several coeval clusters. However, its extension seems to be excessive for the quiet process of dissolution with a typical velocity of 1 pc/Myr [29]. If Group V is a result of some violent process, its members would have spatial velocities indicating this.

In 2019, Jerabkova et al. [30] found a new type of stellar group within the discussed region. They reported the discovery of an "old" stellar "relic filament" associated with a star-forming region in Orion. The structure is distinguished by PM, is located at a distance of ∼430 pc from the Sun, and has a filamentous shape in the sky that is ∼90 pc long. The discovered structure is identified either as a relic filament of Orion with an age of ∼17 million years or as a relic of star formation in a filament of a molecular cloud. The members of the Orion relic filament include ∼100 stars. This may mean the short life of the evolutionary phase after the removal of gas and before the scattering of stars due to tides. The formation of tidal tails and flows in this "model" occurs later.

Probably due to the previously discussed issues with distinguishing between stellar groups in Orion, the authors of [30] did not publish the list of probable members except for the few bright stars for which they obtained radial velocities. Of their 13 Gaia sources, 5 sources are included in our Dataset A, and 4 are included in Dataset B. In spite of the lack of information, based on the figures by [30], one might suggest that the structure they discussed and Group V refer to the same object or its parts. We would like to approach

the nature of Group V by performing backward integration of the orbit of its probable members. Some of them have radial velocities from Gaia DR3, namely 62 stars of the bright Dataset B. The mean error of radial velocities for this sample is $\epsilon_{VR} = 4.6$ km/s, which makes star-by-star orbital integration non-informative. Thus, we use the fact that in space, Group V may be tentatively divided into two subsets (further referred to, according to Figure 4, as "green" and "blue"), as revealed using the clustering algorithm (Section 2.3). We calculated the mean values $(\alpha, \delta, \varpi, \mu_\alpha, \mu_\delta, VR)$ for these two datasets and performed backward integration of the orbit for them. In Table 2, we cite the present-time mean characteristics for the Dataset B members of the "green" and "blue" groups.

Table 2. Mean parameters of the two spatial subsets of Dataset B.

Parameter	Dataset B_{green} *	Dataset B_{blue} *	Units
α	84.28 ± 0.12	83.95 ± 0.06	deg
δ	-4.73 ± 0.24	-1.71 ± 0.09	deg
ϖ	2.370 ± 0.011	2.372 ± 0.007	mas
μ_α	-1.669 ± 0.055	-1.449 ± 0.050	mas/yr
μ_δ	1.263 ± 0.057	0.995 ± 0.042	mas/yr
VR	27.98 ± 1.7	27.99 ± 2.1	km/s

* Cited errors are errors of the mean. Number of stars in the sample B_{green} for VR $N = 16$, and for other parameters, $N = 21$. Number of stars in the sample B_{blue} for VR $N = 44$, and for other parameters, $N = 62$.

The "green" sample includes 21 stars, of which 16 have radial velocities in Gaia DR3. The "blue" sample includes 62 stars, 46 of which have radial velocities in Gaia DR3. Of these 46 radial velocities, we discard two as outliers out of 3σ and proceed with 44 radial velocities for the "blue" sample. We mark stars according to the sample in Table A2.

We generated a set of 1000 Gaussian samples of parameters according to Table 2 for each subset, "green" and "blue". We used the *galpy* package http://github.com/jobovy/galpy, (accessed on 19 April 2023) [31] to integrate the trajectories of each sample backward in time for the maximum time of the expected age of Group V, 16 Myr. The resulting difference in the position of "green" and "blue" subsets is presented in Table 3. The estimation of the expected difference for the initial position of the subsets (16 Myr ago) is half that of the present distance. On the other hand, uncertainties of initial coordinates are large and dominated by uncertainties in velocities.

Table 3. Evolution of relative position of the two spatial subsets of Dataset B.

Dimension, pc	Present **	−16 Myr **
ΔX *	12 ± 2	5 ± 38
ΔY *	-17 ± 2	-6 ± 19
ΔZ *	-8 ± 1	6 ± 11
Distance	22 ± 3	10 ± 44

* Difference in Galactic coordinates is given as $\Delta X = \bar{X}_{green} - \bar{X}_{blue}$, $\Delta Y = \bar{Y}_{green} - \bar{Y}_{blue}$, $\Delta Z = \bar{Z}_{green} - \bar{Z}_{blue}$. ** Cited errors are obtained as mean squared error of 1000 models (see text).

The estimation of the expected difference for the initial position of the subsets (16 Myr ago) is half that of the present distance. This corresponds to the slow dissolution of the system with a rate of some 0.8 pc/Myr. Uncertainties of coordinates back to 16 Myr are large and dominated by uncertainties in velocities.

This result suggesting a slow dissolution may support the hypothesis by [30] about the relic of the stellar filament.

If, on the other hand, we take into account the dispersion of radial velocities $\sigma_{VR} \approx 11$ km/s, then we should suppose that the structure must be in a state of rapid dissolution.

For a scattered stellar structure of unknown scale and form, it is difficult to discover its full extension. There is a subtle balance between neglecting probable members and accepting contaminating sources. This is especially relevant when the surrounding stars are

so similar in kinematics and evolutionary stage as in Orion. In the present investigation, we do not uncover the full extent of Group V; however, by increasing the field of search, one also increases the fraction of contaminating sources and smears the picture (as seen from the comparison of Figure 1 (bottom-left panel) and Figure 1 (bottom-right panel)). At present, one may expect that one of the major sources of contamination is physically bound close binary pairs Gulliver 6 and UBC 17b [32], located in proximity to Group V. The members of these two systems differ in mean kinematical properties but are intermingled in space (Figure 6). With respectto age, these clusters and Group V are are very much alike.

5. Conclusions

Using the Gaia DR3 data, we find the group of stars (Group V) to share common kinematics. The group includes about 150 to 300 stars. It is located in the vicinity of the Orion A cloud. OSCs NGC 1980, NGC 1977, ONC, NGC 1981, and a double cluster Gulliver 6 + UBC 17b are located close to Group V, within a few tens of parsecs. The present linear size of Group V may be about 60 pc.

The two independently selected lists of probable candidates for Group V are given in Appendix A (Dataset A is limited in parallax, and Dataset B is limited in stellar magnitude). The age of the group, its spatial dimensions, spatial velocity V_s and dispersion ($\bar{V}_s = 28.3$ km/s, $\sigma_{V_s} = 11$ km/s) were determined. We make suggestions about the possible nature of Group V. The spatial velocity of Group V and neighboring clusters coincide within the errors dominated by errors in VR. The spatial velocity dispersion of Group V stars indicates that it is part of a decaying stellar complex. Obviously, we should pay attention to the fact that the radial velocity error for our data is large. According to our estimates, it is approximately 3.0 km/s for stars brighter than $G_{mag} = 14$ and approximately 8.0 km/s for fainter stars. Accounting for such a radial velocity error can reduce the value σ_{V_S} to ∼6 km/s.

On the other hand, mean kinematic characteristics of the two spatially separated subsets of Group V indicate that its dissolution may be quite slow, with a typical rate of less than 1 pc/Myr.

Author Contributions: The idea, S.V., K.L., A.K. and N.K.; methodology, S.V., N.C. and D.K.; software, N.C., D.K., N.K. and S.S.; validation, S.V., N.C. and D.K.; formal analysis, S.V., N.C., K.L., A.K. and N.K.; investigation, S.V., N.C. and D.K.; data curation, N.C. and D.K.; writing—original draft preparation, S.V.; writing—review and editing, S.V., N.C. and D.K.; visualization, N.C.; supervision, S.V.; project administration, S.V. All authors have read and agreed to the published version of the manuscript.

Funding: This research received no external funding.

Data Availability Statement: Data are contained within the article. The tables from the article will be also available via CDS.

Acknowledgments: This work has made use of data from the European Space Agency (ESA) mission Gaia (https://www.cosmos.esa.int/gaia, accessed on 25 January 2023), processed by the Gaia Data Processing and Analysis Consortium (DPAC, https://www.cosmos.esa.int/web/gaia/dpac/consortium, accessed on 25 January 2023). Funding for the DPAC has been provided by national institutions, in particular, the institutions participating in the Gaia Multilateral Agreement. The use of TOPCAT, an interactive graphical viewer and editor for tabular data [33], is acknowledged. This research has made use of the SIMBAD database, operated at CDS, Strasbourg, France [34]. The authors thank the reviewers for their helpful advice and comments.

Conflicts of Interest: The authors declare no conflict of interest.

Appendix A

The Appendix contains the two lists of probable members of Group V (Dataset A and Dataset B). The listed parameters are either from Gaia DR3 (columns marked by *) or calculated by the authors. Extended tables will be available via CDS.

Table A1. Dataset A.

Gaia DR3 Source Id.	ϖ	μ_α	μ_δ	G_{mag}	**BP-RP**	**RV**	ϵ_{VR}	**X**	**Y**	**Z**	**U**	**V**	**W**	A_G	E_{BP-RP}
Gaia DR3 Source Id. *	ϖ *	μ_α *	μ_δ *	G_{mag} *	**BP-RP ***	**VR ***	ϵ_{VR} *	**X**	**Y**	**Z**	**U**	**V**	**W**	A_G *	E_{BP-RP} *
	mas	**mas/yr**		**mag**		**km/s**			**pc**			**km/s**		**mag**	
3010622094238648448	2.3744	−1.676	1.072	11.964	0.756	50.65	1.12	−326.8	−218.8	−150.6	40.5	−23.1	−20.1	0.160	0.086
3012148010219208832	2.3674	−1.891	1.517	19.924	2.406			−330.3	−218.8	−146.5					
3013842941753415424	2.3719	−2.059	1.126	19.292	2.823			−328.5	−206.6	−164.9					
3014860337903007616	2.4697	−1.783	1.442	19.925	2.951			−322.8	−192.8	−150.2					
3014941426886464256	2.4371	−2.109	1.363	17.614	2.414			−325.1	−191.9	−160.7				0.524	0.318
3015433488402344576	2.4025	−1.734	1.164	20.785	1.498			−332.6	−208.6	−138.2					
3016010525849058304	2.4679	−1.784	1.361	20.621	2.880			−325.5	−200.7	−134.2					
3016071827917538048	2.3365	−2.136	1.365	12.190	0.799	−2.13	2.33	−346.4	−210.1	−138.0	−0.2	5.3	−1.8	0.136	0.074
3016111650854337408	2.3449	−1.617	1.399	15.072	1.787	36.44	8.59	−344.8	−208.9	−139.1	31.1	−14.2	−13.5	0.912	0.490
3016216856077986688	2.3334	−1.828	1.327	10.461	0.508	23.57	3.56	−347.7	−209.7	−137.0	20.6	−7.7	−9.6		
3016825160886293120	2.4647	−2.112	1.338	18.121	3.220			−330.9	−188.1	−140.6				0.801	0.590
3016900103770771456	2.3709	−1.426	1.551	17.579	2.965			−343.5	−203.3	−136.3				0.959	0.631
3016913156175056768	2.336	−1.782	1.499	17.912	3.033			−348.9	−205.6	−138.9				1.120	0.741
3016970536938230272	2.4103	−1.893	1.148	18.730	3.272			−339.1	−197.0	−135.4					
3016987476288866048	2.3647	−1.597	1.591	12.506	0.897	32.45	2.87	−346.0	−199.4	−139.0	28.3	−11.4	−12.0	0.482	0.261
3017007198779743104	2.3251	−1.818	1.33	17.705	3.144			−350.7	−206.4	−139.2				1.599	1.013
3017016475908135808	2.3555	−1.821	1.073	16.903	2.688			−346.9	−203.8	−135.5				0.682	0.433
3017060215858357376	2.325	−1.555	0.959	18.868	3.184			−351.4	−204.8	−139.8					
3017065580271198976	2.3259	−1.615	1.381	16.306	2.369			−351.7	−203.8	−140.0				0.631	0.376
3017078465173084032	2.3642	−1.594	1.156	18.411	3.276			−346.4	−199.9	−137.6				1.412	0.964
3017084443767558272	2.4018	−1.637	1.339	13.737	1.278	28.94	2.11	−341.4	−196.0	−135.6	25.1	−10.0	−11.0	0.382	0.204
3017084443767558400	2.3595	−1.889	1.485	17.365	2.850			−347.5	−199.5	−138.0				0.980	0.633
3017085440199967232	2.413	−2.056	1.39	15.961	2.266			−340.0	−194.9	−134.8				0.986	0.557
3017086711510771328	2.3399	−1.563	1.332	17.189	2.785			−350.5	−201.9	−137.9				0.761	0.493
3017181063353045248	2.4852	−1.883	1.238	17.525	2.868			−329.9	−188.2	−132.9				1.021	0.658
3017318983354345088	2.3651	−1.66	1.534	14.082	1.499	17.85	5.22	−349.2	−198.0	−132.8	16.4	−4.4	−7.1	1.196	0.642
3017327092252520448	2.3177	−1.87	1.014	16.703	2.591			−356.0	−200.6	−138.4				1.182	0.690
3017341523342707968	2.3356	−1.412	1.328	16.069	2.421			−352.2	−198.2	−141.5				3.317	1.874
3017370626039362048	2.3856	−1.629	1.341	19.040	3.331			−346.5	−192.3	−136.6					
3017387118715416960	2.3319	−2.003	0.882	13.584	1.357	36.83	3.52	−355.1	−197.7	−136.9	31.4	−13.5	−14.4	1.168	0.637
3017390623408731520	2.376	−1.493	1.295	16.828	2.653			−348.7	−193.6	−134.6				0.925	0.566
3017401515444135040	2.3949	−1.575	1.379	17.759	3.199			−346.1	−190.8	−134.7				1.605	1.038
3017403920625813120	2.4033	−1.629	1.344	19.188	3.260			−345.0	−190.7	−133.2					

Table A1. *Cont.*

Gaia DR3 Source Id.	ϖ	μ_α	μ_δ	G_{mag}	BP-RP	RV	ϵ_{VR}	X	Y	Z	U	V	W	A_G	E_{BP-RP}
Gaia DR3 Source Id. *	ϖ *	μ_α *	μ_δ *	G_{mag} *	BP-RP *	VR *	ϵ_{VR} *	X	Y	Z	U	V	W	A_G *	E_{BP-RP} *
	mas	mas/yr		mag		km/s		pc			km/s			mag	
3017406875563305728	2.4822	−1.573	1.463	17.633	3.385			−334.4	−184.3	−128.6				1.445	1.001
3017407184800946944	2.3419	−1.83	1.473	17.845	3.149			−354.5	−195.1	−136.2				1.325	0.911
3017407940715202816	2.4055	−1.83	1.46	12.376	1.052	26.02	3.13	−344.9	−189.9	−133.4	23.1	−7.9	−10.2		
3023162715844336128	2.3736	−1.873	1.44	14.186	1.526	62.11	4.96	−349.5	−199.1	−125.4	53.1	−25.4	−20.4	0.731	0.396
3023275243987425792	2.4087	−1.914	1.6	17.525	3.136			−345.3	−194.7	−123.3				0.986	0.672
3023354851204687744	2.3742	−2.106	0.942	18.349	3.225			−349.6	−194.8	−131.2				1.127	0.763
3023411171112882816	2.4291	−1.698	1.472	16.952	2.715			−341.9	−188.4	−130.7				1.032	0.634
3023413984315736704	2.375	−1.786	1.342	18.463	3.188			−350.0	−192.6	−133.1					
3023413988611422720	2.3377	−1.59	1.657	16.406	2.423			−355.6	−195.7	−135.2				0.856	0.502
3023496894363769216	2.465	−1.878	1.075	18.390	3.160			−339.4	−187.4	−119.5				1.223	0.849
3023980305817582976	2.3582	−1.564	0.972	18.820	2.459			−357.6	−192.7	−121.6					
3025392040093020800	2.3999	−1.908	1.447	20.463	1.488			−353.8	−194.8	−102.4					
3025654174832036224	2.4849	−1.45	1.117	20.585	2.221			−343.3	−183.7	−101.5					
3208739521035049984	2.4155	−1.684	1.154	20.632	1.130			−339.8	−170.0	−164.4					
3209446854905159040	2.3168	−1.647	1.139	16.348	2.502			−357.0	−194.3	−145.2				3.074	1.706
3209512275846903040	2.3617	−1.714	1.457	17.833	3.167			−350.9	−188.4	−143.8				1.217	0.810
3209541687784992384	2.3838	−1.846	1.254	11.204	1.101	19.71	5.88	−347.2	−188.6	−140.9	17.5	−5.1	−8.6		
3209555427381596928	2.3551	−1.584	1.104	18.175	3.437			−352.1	−193.0	−138.2				2.348	1.447
3209556565551727232	2.4868	−1.522	1.58	17.075	3.052			−333.7	−182.9	−130.0				1.610	0.997
3209557287106237056	2.3723	−1.675	1.461	16.017	2.254			−349.7	−191.3	−137.0					
3209566632955057664	2.4965	−1.789	1.536	17.662	3.052			−333.1	−181.7	−128.4				1.517	0.959
3209566632955057920	2.4742	−1.462	1.511	17.483	3.043			−336.1	−183.3	−129.5				1.637	1.011
3209640197154658304	2.4987	−2.011	0.879	16.637	2.542			−333.9	−178.5	−129.6				0.559	0.350
3209656552390066688	2.3708	−1.737	1.393	13.903	1.333	26.08	2.66	−352.3	−186.4	−137.9	23.2	−7.7	−10.2	0.414	0.223
3209776914552420480	2.3344	−1.563	1.092	13.692	1.395	16.36	5.95	−356.6	−185.8	−147.7	14.7	−3.8	−7.3	0.709	0.384
3209830756262184832	2.4321	−1.434	1.123	17.845	3.452			−342.9	−179.3	−139.1				3.433	1.917
3209838418483918592	2.4037	−1.914	1.401	17.296	2.939			−347.3	−183.2	−137.5				0.954	0.633
3209838899520253056	2.4034	−1.749	1.259	16.283	2.340			−347.5	−183.0	−137.5				0.795	0.460
3209839002599466880	2.3278	−1.895	1.341	16.870	2.709			−358.7	−189.1	−141.8				0.876	0.549
3210110302796747648	2.4222	−1.815	1.787	11.638	0.709	6.75	0.85	−341.0	−175.2	−153.1	7.2	1.6	−3.9		
3210144353298268160	2.3865	−2.171	1.55	19.953	2.237			−347.3	−177.5	−153.1					
3210169848224432000	2.4599	−1.856	1.328	20.811	1.586			−335.8	−169.8	−153.8					
3210693559355787264	2.4524	−1.998	0.883	16.970	2.911			−343.1	−173.2	−136.2					

Table A1. *Cont.*

Gaia DR3 Source Id.	ϖ	μ_α	μ_δ	G_{mag}	BP-RP	RV	ϵ_{VR}	X	Y	Z	U	V	W	A_G	E_{BP-RP}
Gaia DR3 Source Id. *	ϖ *	μ_α *	μ_δ *	G_{mag} *	BP-RP *	VR *	ϵ_{VR} *	X	Y	Z	U	V	W	A_G *	E_{BP-RP} *
	mas	mas/yr		mag		km/s		pc			km/s			mag	
3210728984246548992	2.3481	−1.649	1.562	20.887	2.259			−357.9	−177.9	−147.2					
3215628098822109824	2.3976	−1.842	1.09	18.398	3.023			−349.2	−187.2	−130.3				0.663	0.474
3215676138032548224	2.4295	−1.901	1.144	18.563	1.805			−344.8	−184.0	−129.3				0.002	0.001
3215676138032548480	2.3736	−1.688	1.321	16.635	2.541			−352.9	−188.3	−132.3					
3215679123033701888	2.3796	−1.802	1.195	18.420	3.259			−352.3	−187.6	−131.4				0.596	0.445
3215694000802887552	2.3718	−1.537	1.283	17.847	3.060			−353.8	−187.2	−132.6					
3215832818437324800	2.3666	−2.031	1.106	20.553	1.090			−357.8	−187.6	−123.9					
3215861057848075392	2.4024	−1.587	1.159	12.062	0.899	34.55	5.11	−349.1	−183.3	−133.3	30.1	−11.9	−12.7	0.228	0.123
3215878134638733824	2.4381	−1.869	1.067	17.935	2.935			−344.4	−179.3	−132.1				0.777	0.526
3215944178351833472	2.42	−1.918	1.344	18.453	3.313			−347.7	−177.0	−136.2				0.943	0.659
3215945140425054848	2.4134	−1.765	1.448	11.030	0.582	28.2	1.08	−348.7	−177.1	−136.9	25.1	−8.1	−11.0		
3215948507678807168	2.3943	−1.941	1.089	17.421	2.213			−351.8	−179.7	−135.7				0.479	0.279
3216001864056373760	2.4698	−1.94	0.875	19.611	3.113			−342.1	−178.1	−123.3					
3216051513882385280	2.4867	−1.676	1.162	19.388	3.047			−341.3	−174.0	−122.4					
3216054954147675392	2.3666	−1.504	1.543	12.471	0.807	29.8	2.4	−358.9	−183.8	−126.4	26.9	−9.1	−10.1	0.122	0.066
3216061443842831872	2.4367	−2.206	1.421	12.277	0.819	26.94	3.82	−349.1	−177.8	−122.4	24.3	−7.4	−10.4	0.194	0.105
3216087595899052800	2.4759	−1.687	0.935	18.083	3.238			−342.7	−172.7	−125.9				0.792	0.557
3216090516476803456	2.3237	−1.515	1.145	10.518	0.223	27.08	3.62	−365.2	−184.1	−133.8	24.1	−8.2	−10.0		
3216096632510194176	2.3779	−1.621	1.444	13.134	1.007	29.46	1.53	−357.5	−179.4	−129.7	26.4	−8.7	−10.5	0.179	0.095
3216101339793412352	2.4465	−2.066	1.446	20.778	1.424			−347.3	−176.3	−124.0					
3216104049917812608	2.3899	−1.98	1.38	15.187	1.836	34.97	9.73	−355.6	−179.7	−127.8	31.0	−10.9	−12.8	0.344	0.187
3216109242534289664	2.4788	−1.956	1.014	10.629	0.335	30.62	1.75	−343.2	−174.1	−121.0	27.0	−9.8	−11.5	0.165	0.088
3216119687894593664	2.4151	−1.662	1.271	19.071	3.253			−352.5	−176.9	−126.2					
3216138826268839936	2.3371	−2.109	1.459	16.554	2.520			−361.4	−192.6	−124.0				1.239	0.711
3216204586512307072	2.3707	−2.286	1.358	17.497	2.936			−357.0	−187.8	−123.3				0.835	0.551
3216371750933759104	2.3709	−1.843	0.984	20.247	3.275			−360.5	−185.6	−116.2					
3216392023179484160	2.4549	−1.649	0.873	20.671	1.968			−349.1	−180.4	−107.3					
3216437442459796992	2.3899	−1.798	1.445	17.355	2.825			−356.2	−181.2	−124.1				0.802	0.529
3216442291478386688	2.4038	−2.151	1.538	14.183	1.403	47.29	5.61	−354.5	−180.5	−121.7	41.8	−16.1	−16.1	0.427	0.229
3216444387422405632	2.3206	−1.995	1.497	17.121	2.789			−367.4	−187.1	−125.3				0.7819	0.5075
3216485069352710912	2.354	−1.968	1.436	13.252	1.164	23.69	3.12	−361.7	−183.5	−126.4	21.6	−6.0	−9.1	0.273	0.147
3216494312121076096	2.4579	−1.761	1.585	16.866	2.828			−347.1	−175.6	−119.3					
3216526678995624448	2.3979	−2.082	0.893	17.177	2.869			−356.9	−178.5	−121.0					

Table A1. *Cont.*

Gaia DR3 Source Id.	ϖ	μ_α	μ_δ	G_{mag}	BP-RP	RV	ϵ_{VR}	X	Y	Z	U	V	W	A_G	E_{BP-RP}
Gaia DR3 Source Id. *	ϖ *	μ_α *	μ_δ *	G_{mag} *	BP-RP *	VR *	ϵ_{VR} *	X	Y	Z	U	V	W	A_G *	E_{BP-RP} *
	mas	mas/yr		mag		km/s		pc			km/s			mag	
3216805641421533312	2.3677	−2.024	1.261	17.564	2.980			−358.6	−176.5	−136.5				1.118	0.728
3216837531549482880	2.3564	−1.52	1.149	13.796	1.261	45.01	3.67	−360.1	−180.6	−133.5	39.3	−15.8	−15.7	0.379	0.203
3216838665419654912	2.3602	−1.476	1.639	17.300				-359.7	−180.0	−133.3					
3216843888100939008	2.4001	−1.374	1.04	14.774	1.710	20.97	4.48	−354.0	−176.4	−131.0	18.8	−5.9	−8.0	0.472	0.252
3216844437857284480	2.3935	−1.448	0.976	16.754	1.933			−355.2	−176.8	−130.9					
3216850313372144000	2.3433	−1.832	1.02	11.776	0.696	25.86	2.7	−362.8	−180.6	−133.6	22.9	−7.4	−10.3	0.215	0.116
3216874051655373440	2.3802	−1.865	1.267	18.976	3.177			−357.9	−178.1	−129.1				0.412	0.323
3216876254974564352	2.442	−1.78	1.712	18.310	3.091			−349.2	−173.6	−125.1				0.966	0.668
3216895908744725632	2.4026	−1.578	1.504	14.698	1.612			−355.3	−174.3	−129.0				0.192	0.102
3216897622436254336	2.3219	−1.429	1.148	17.923	3.090			−367.8	−180.2	−133.1				0.750	0.542
3216897691155023360	2.3346	−1.309	1.386	13.716	1.299	−36.47	6.21	−365.9	−179.3	−132.1	−29.8	18.8	10.3	0.907	0.490
3216919990625228416	2.3749	−1.469	0.967	11.603	0.669	30.95	2.81	−359.4	−175.7	−131.4	27.3	−9.9	−11.3	0.157	0.084
3216937758905876352	2.3806	−1.503	1.195	16.898	2.826			−359.1	−173.6	−131.9				0.861	0.555
3216947413992534272	2.4079	−1.405	1.225	17.339	2.711			−354.9	−172.9	−128.9				0.858	0.565
3216954487801986048	2.375	−1.525	1.11	17.818	3.077			−360.4	−175.5	−128.9				0.867	0.592
3216966518006856448	2.4136	−1.706	1.379	14.287	1.464	−6.73	5.29	−354.6	−171.0	−129.0	−4.5	6.6	0.5	0.507	0.271
3216997407412184448	2.3776	−1.378	1.217	9.1413	−0.033	25.69	26.72	−357.0	−171.8	−141.3	22.9	−7.2	−9.8		
3217028296817018752	2.3844	−2.13	1.122	15.822	2.266			−357.7	−171.9	−135.7				0.507	0.297
3217274823643738752	2.4181	−2.239	1.155	19.397	3.427			−354.4	−174.6	−122.2					
3217290633419229056	2.4771	−1.914	0.824	18.124	3.134			−346.2	−169.0	−120.5				0.638	0.449
3217332135686020224	2.3468	−2.073	1.093	17.634	3.019			−365.4	−178.0	−128.1				0.818	0.558
3217332174343645696	2.3647	−2.102	1.152	10.101	0.233			−362.6	−176.5	−127.2				0.743	0.399
3217347601865296512	2.3729	−2.118	1.15	11.728	0.884	29.43	2.52	−361.6	−174.5	−128.2	26.3	−8.2	−11.5	0.234	0.125
3217347735007460992	2.4695	−1.447	1.048	19.052	3.409			−347.5	−167.7	−122.9					
3217350105829476992	2.4141	−1.664	1.135	16.597	2.848			−355.8	−171.3	−125.1				0.774	0.513
3217350900398106240	2.4929	−1.533	1.55	16.366				-344.6	−165.6	−121.4					
3217356015703988864	2.4253	−1.728	0.995	8.6315	0.041	23.35	3.62	−354.2	−170.5	−124.4	20.9	−6.4	−9.0	0.240	0.128
3217356909057734912	2.3663	−1.477	1.147	17.892	3.153			−363.2	−174.5	−127.5				0.663	0.458
3217359657837224704	2.348	−1.905	1.674	20.151	2.801			−366.4	−175.7	−127.4					
3217362303536988928	2.4148	−1.449	1.301	18.909	3.352			−356.4	−170.0	−124.7				0.238	0.190
3217387837118879488	2.3891	−1.568	1.45	14.987	1.723	18.6	9.11	−360.6	−171.9	−124.9	17.4	−3.9	−6.9	0.418	0.223
3217391273090887168	2.4493	−1.874	0.965	16.171	2.742			−351.9	−168.6	−120.1					

Table A1. *Cont.*

Gaia DR3 Source Id.	ϖ	μ_α	μ_δ	G_{mag}	**BP-RP**	**RV**	ϵ_{VR}	**X**	**Y**	**Z**	**U**	**V**	**W**	A_G	E_{BP-RP}
Gaia DR3 Source Id. *	ϖ *	μ_α *	μ_δ *	G_{mag} *	**BP-RP ***	**VR ***	ϵ_{VR} *	**X**	**Y**	**Z**	**U**	**V**	**W**	A_G *	E_{BP-RP} *
	mas	**mas/yr**			**mag**	**km/s**			**pc**			**km/s**			**mag**
3217445183521903232	2.3292	−1.756	1.103	13.353	1.920	−22.61	21.67	−371.0	−180.9	−118.0	−18.5	13.1	4.2		
3217512730471453952	2.485	−1.899	1.308	16.609	3.007			−348.7	−166.5	−112.3				0.718	0.495
3217556199837262464	2.4392	−2.123	1.253	16.039	2.339			−353.3	−167.2	−123.7				0.686	0.406
3217571696079288192	2.4314	−1.654	1.358	12.400	1.098	28.33	3.74	−354.7	−166.4	−125.2	25.6	−7.8	−10.1	0.609	0.330
3217581724826579072	2.38	−1.559	1.125	17.524	2.887			−362.6	−171.2	−125.6				0.701	0.472
3217636395466272000	2.3513	−1.416	0.982	15.764	2.531			−367.5	−168.7	−131.9					
3217640067664459520	2.4242	−1.778	1.153	17.337	3.037			−356.8	−164.7	−125.4				0.843	0.576
3217651032714904576	2.3369	−1.341	1.299	16.764	2.514			−370.1	−171.6	−129.1				0.569	0.355
3217691302328206080	2.3283	−1.603	1.04	13.726	1.196	24.7	7.18	−372.1	−175.3	−123.6	22.4	−6.8	−8.9	0.351	0.188
3217729269838908032	2.3958	−1.836	1.193	15.106	1.129			−363.2	−170.0	−115.7					
3217746758945744256	2.358	−1.642	1.434	18.410	3.139			−369.5	−171.3	−118.3				0.960	0.686
3217758608758824960	2.4595	−1.888	0.861	18.022	2.990			−353.1	−162.7	−119.0				0.915	0.624
3217759295954420480	2.3319	−1.691	1.071	19.570	3.036			−372.4	−171.4	−125.8					
3217761739789728896	2.3191	−1.979	1.291	20.593				−374.6	−172.8	−125.5					
3217767095614328960	2.4058	−1.37	1.51	16.518	2.805			−361.5	−166.4	−120.1				0.710	0.468
3220106615839694848	2.3787	−1.824	1.138	18.986	1.072			−359.7	−164.5	−142.6				0.168	0.092
3220310987564302592	2.4337	−2.0	1.713	20.275	2.293			−354.6	−157.5	−135.4					
3220685650446800384	2.4248	−1.587	1.073	12.832	1.079	19.42	8.12	−358.3	−162.3	−123.9	17.8	−4.4	−7.5	0.469	0.251
3220687437153177088	2.3612	−1.815	1.184	16.522	2.8894			−368.2	−166.7	−126.6				0.793	0.527

* Data from Gaia DR3.

Table A2. Dataset B.

Gaia DR3 Source Id.	ϖ	μ_α	μ_δ	G_{mag}	**BP-RP**	**VR**	ϵ_{VR}	VR_{exp}	P_{tot}	**X**	**Y**	**Z**	**Flag**
Gaia DR3 Source Id. *	ϖ *	μ_α *	μ_δ *	G_{mag} *	**BP-RP ***	**VR ***	ϵ_{VR} *	VR_{exp} **	P_{tot} ***	**X**	**Y**	**Z**	**Flag**
	mas	**mas/yr**	**mas/yr**	**mag**	**mag**	**km/s**	**km/s**	**km/s**		**pc**	**pc**	**pc**	********
3216953014630150016	2.3064	−1.581	0.719	14.913	1.761	39.94	6.26	27.90	0.93	−371.0	−180.7	−132.7	B
3216953083349306240	2.3070	−1.498	0.746	14.847	1.676	-22.62	10.15	27.90	0.96	−370.9	−180.5	−132.9	B
3216946310184034816	2.3460	−1.330	1.050	15.746	2.150			27.90	0.99	−364.4	−177.8	−131.3	B
3216949917956299648	2.3116	−1.477	0.927	11.806	0.827	31.33	1.55	27.91	0.98	−370.0	−179.9	−133.4	B
3216897691155023360	2.3345	−1.308	1.385	13.716	1.299	-36.47	6.21	27.90	0.89	−365.8	−179.3	−132.0	BO
3216895908744725632	2.4025	−1.578	1.504	14.698	1.612			27.90	0.84	−355.2	−174.2	−128.9	B
3215983485892366976	2.3118	−1.425	1.104	11.383	0.729	26.46	3.46	27.88	0.98	−365.9	−184.4	−138.4	G

Table A2. *Cont.*

Gaia DR3 Source Id.	ϖ	μ_α	μ_δ	G_{mag}	BP-RP	VR	ϵ_{VR}	VR_{exp}	P_{tot}	X	Y	Z	Flag
Gaia DR3 Source Id. *	ϖ * mas	μ_α * mas/yr	μ_δ * mas/yr	G_{mag} * mag	BP-RP * mag	VR * km/s	ϵ_{VR} * km/s	VR_{exp} ** km/s	P_{tot} ***	X pc	Y pc	Z pc	Flag ****
3017298401871010816	2.2951	−1.563	1.147	15.813	2.384			27.70	0.76	−358.7	−202.8	−141.2	G
3215918580346776832	2.4548	−1.805	0.666	14.950	1.735	9.43	5.73	27.84	0.68	−343.8	−177.0	−128.0	G
3216090516476803456	2.3237	−1.515	1.144	10.518	0.223	27.08	3.61	27.87	0.94	−365.2	−184.1	−133.7	B
3216837531549482880	2.3564	−1.519	1.148	13.796	1.261	45.01	3.67	27.88	0.80	−360.1	−180.5	−133.4	B
3215928063634719616	2.4235	−1.225	0.720	15.381	1.920			27.87	0.72	−346.9	−177.8	−135.1	G
3216843888100939008	2.4001	−1.373	1.040	14.774	1.710	20.96	4.47	27.89	0.99	−354.0	−176.3	−130.9	B
3215861057848075392	2.4024	−1.587	1.159	12.062	0.899	34.55	5.11	27.82	0.93	−349.1	−183.3	−133.2	G
3215898892217219200	2.3070	−1.550	1.547	15.730	2.087			27.82	0.95	−365.1	−190.3	−135.3	G
3215945140425054848	2.4133	−1.764	1.447	11.030	0.582	28.19	1.07	27.88	0.81	−348.6	−177.1	−136.9	G
3216109242534289664	2.4788	−1.956	1.013	10.629	0.335	30.61	1.74	27.84	0.93	−343.1	−174.1	−121.0	B
3216485069352710912	2.3540	−1.967	1.436	13.252	1.164	23.68	3.12	27.83	0.85	−361.6	−183.5	−126.3	B
3216842616790661120	2.3201	−1.022	0.481	11.461	0.694	9.18	10.13	27.89	0.70	−365.9	−182.1	−136.6	B
3216871101013663360	2.3021	−1.360	0.669	13.777	1.332	20.90	3.24	27.90	0.91	−370.3	−182.0	−135.5	B
3215637689485259904	2.5013	−1.957	1.328	13.217	1.242	39.89	4.26	27.78	0.92	−335.3	−178.8	−124.0	G
3217785104413698432	2.2983	−0.955	1.031	15.864	2.144			27.94	0.72	−378.9	−172.5	−126.1	B
3217771360518389888	2.3087	−1.207	0.796	15.489	1.983			27.94	0.94	−376.2	−172.6	−127.3	B
3215804501717947648	2.3595	−1.339	1.514	11.374	0.594	29.06	1.76	27.81	0.89	−357.1	−186.8	−130.9	G
3217778163746565248	2.4270	−0.765	0.342	12.053	0.811	24.30	3.38	27.94	0.64	−358.3	−164.0	−120.1	B
3217776342680441600	2.4344	−0.695	0.849	13.524	1.293	35.21	5.35	27.94	0.62	−357.2	−162.9	−120.5	B
3215781794227643392	2.3318	−2.232	0.900	13.593	1.356	32.54	5.54	27.78	0.65	−360.4	−191.6	−131.3	G
3209656552390066688	2.3707	−1.737	1.392	13.903	1.333	26.08	2.65	27.82	0.89	−352.3	−186.4	−137.8	G
3017300360376086912	2.3041	−1.316	1.406	12.942	1.151	27.55	3.15	27.70	0.88	−357.6	−202.1	−140.0	G
3017084443767558272	2.4018	−1.637	1.339	13.737	1.278	28.94	2.11	27.67	0.78	−341.3	−196.0	−135.5	G
3016995142807726080	2.3023	−1.734	1.271	15.517	1.986			27.62	0.70	−354.0	−208.8	−140.3	G
3017318983354345088	2.3650	−1.659	1.534	14.082	1.499	17.85	5.22	27.68	0.96	−349.1	−197.9	−132.8	G
3216919410805808128	2.3562	−1.239	1.801	14.934	1.823	50.61	7.11	27.91	0.65	−362.1	−177.1	−132.6	B
3216919990625228416	2.3748	−1.469	0.967	11.603	0.669	30.95	2.80	27.91	0.94	−359.3	−175.7	−131.3	B
3215847898068343936	2.3574	−2.256	0.882	11.565	0.707	25.14	1.79	27.80	0.74	−359.3	−187.0	−125.8	B
3216052445886802048	2.3392	−2.194	0.628	10.628	0.552	31.72	1.15	27.83	0.63	−362.9	−185.5	−128.7	B
3216442291478386688	2.4037	−2.150	1.538	14.183	1.403	47.29	5.60	27.82	0.77	−354.4	−180.5	−121.6	B
3217636395466272000	2.3512	−1.415	0.982	15.764	2.531			27.97	0.93	−367.4	−168.6	−131.8	B
3220685650446800384	2.4247	−1.587	1.073	12.832	1.079	19.41	8.11	27.96	0.83	−358.2	−162.3	−123.9	B
3220701043609564928	2.3717	−1.093	0.849	13.772	1.339	24.88	3.60	27.97	0.91	−366.8	−165.1	−126.1	B
3217626976602419712	2.4354	−1.503	0.236	15.687	2.347			27.95	0.81	−354.9	−164.7	−124.4	B

Table A2. *Cont.*

Gaia DR3 Source Id.	ϖ	μ_α	μ_δ	G_{mag}	BP-RP	VR	ϵ_{VR}	VR_{exp}	P_{tot}	X	Y	Z	Flag
Gaia DR3 Source Id. *	ϖ * mas	μ_α * mas/yr	μ_δ * mas/yr	G_{mag} * mag	BP-RP * mag	VR * km/s	ϵ_{VR} * km/s	VR_{exp} ** km/s	P_{tot} ***	X pc	Y pc	Z pc	Flag ****
3217387837118879488	2.3891	−1.568	1.449	14.987	1.723	18.59	9.11	27.91	0.75	−360.6	−171.9	−124.8	B
3217649005490309120	2.4578	−1.977	0.380	15.934	2.744			27.93	0.75	−352.0	−163.8	−121.4	B
3217646600308651008	2.3759	−1.057	0.951	14.950	1.663	50.72	7.58	27.94	0.88	−363.8	−169.5	−126.5	B
3217595576097368576	2.3838	−0.787	1.284	10.905	0.412	27.72	1.55	27.92	0.60	−362.3	−170.4	−125.0	B
3217571696079288192	2.4313	−1.653	1.358	12.400	1.098	28.33	3.74	27.94	0.77	−354.6	−166.4	−125.1	B
3217576643881536896	2.4746	−1.160	0.736	14.933	2.035	24.46	7.23	27.91	0.84	−348.4	−165.5	−120.2	B
3217581037633478656	2.3349	−1.801	0.711	12.055	0.835	31.05	3.82	27.92	0.84	−369.5	−174.6	−127.7	B
3217666593380085376	2.3507	−1.151	0.817	9.7916	0.113	22.19	3.51	27.95	0.95	−368.6	−169.7	−127.5	B
3217673126026621440	2.3111	−1.409	0.831	7.9883	0.005	28.77	1.50	27.94	0.97	−375.2	−172.6	−128.8	B
3017085440199967232	2.4130	−2.055	1.390	15.961	2.266			27.68	0.71	−339.9	−194.9	−134.7	G
3016987476288866048	2.3647	−1.596	1.591	12.506	0.897	32.45	2.86	27.67	0.63	−346.0	−199.4	−138.9	G
3017407940715202816	2.4054	−1.829	1.460	12.376	1.052	26.02	3.12	27.75	0.91	−344.9	−189.9	−133.4	G
3215683697174962688	2.4021	−1.317	0.942	10.886	0.412	34.20	3.62	27.80	0.80	−349.3	−185.0	−130.5	G
3217364197618885760	2.4049	−1.712	0.682	15.618	2.082			27.91	0.94	−358.0	−170.8	−124.4	B
3217360207592650240	2.3119	−1.816	0.791	14.876	2.049	46.20	9.67	27.91	0.64	−371.7	−178.1	−130.7	B
3217360452407423232	2.3452	−0.880	1.310	13.783	1.271	24.98	3.23	27.91	0.70	−366.6	−175.5	−128.7	B
3217356015703988864	2.4253	−1.728	0.995	8.6315	0.041	23.35	3.62	27.91	0.95	−354.2	−170.4	−124.3	B
3217547060146911104	2.4208	−1.072	0.811	15.463	2.035	96.12	11.55	27.93	0.92	−355.2	−168.8	−126.1	BO
3217545170361327232	2.3627	−1.293	1.026	14.688	1.568	42.24	8.03	27.93	0.87	−363.7	−172.9	−130.0	B
3217350900400166144	2.4225	−1.337	1.556	14.885	1.776			27.91	0.73	−354.6	−170.4	−124.9	B
3217332174343645696	2.3647	−2.102	1.151	10.101	0.233			27.89	0.74	−362.6	−176.5	−127.2	B
3217336950346568448	2.3241	−1.483	0.774	10.972	0.450	32.78	1.76	27.90	0.98	−369.3	−178.7	−129.5	B
3217184083870448384	2.4404	−0.893	0.921	10.152	0.151	23.92	2.64	27.94	0.86	−352.4	−166.2	−126.5	B
3216969846604549376	2.3531	−1.464	0.755	12.487	1.008	36.75	4.16	27.92	0.96	−363.9	−175.7	−131.2	B
3217347601865296512	2.3729	−2.118	1.150	11.728	0.884	29.42	2.51	27.91	0.69	−361.5	−174.4	−128.1	B
3217350556802789376	2.3250	−1.533	0.712	15.946	2.269			27.91	0.96	−369.3	−177.5	−130.5	B
3216966518006856448	2.4135	−1.705	1.379	14.287	1.464	−6.72	5.29	27.92	0.82	−354.6	−171.0	−129.0	B
3216974386386913408	2.3612	−1.040	0.825	13.286	1.209	25.29	4.06	27.92	0.92	−363.0	−174.3	−130.9	B
3217134262249922304	2.4019	−0.856	0.560	9.0148	0.031	20.70	2.95	27.94	0.78	−356.3	−170.3	−131.4	B
3017291736081784832	2.3040	−1.876	1.323	11.215	0.552	30.89	1.83	27.70	0.77	−356.9	−202.0	−141.8	G
3016216856077986688	2.3333	−1.827	1.326	10.461	0.508	23.56	3.56	27.56	0.66	−347.7	−209.6	−137.0	G
3217584615340797568	2.3859	−0.797	1.084	10.149	0.223	17.83	3.45	27.91	0.64	−361.8	−171.7	−123.4	B
3217382305201141760	2.3439	−1.832	0.744	15.053	1.816	57.13	10.58	27.90	0.91	−367.2	−176.4	−126.6	B
3217371511946673920	2.3136	−1.665	1.416	15.503	2.159			27.89	0.76	−372.0	−179.2	−127.5	B

Table A2. *Cont.*

Gaia DR3 Source Id.	ϖ	μ_α	μ_δ	G_{mag}	**BP-RP**	**VR**	ϵ_{VR}	VR_{exp}	P_{tot}	**X**	**Y**	**Z**	**Flag**
Gaia DR3 Source Id. *	ϖ * **mas**	μ_α * **mas/yr**	μ_δ * **mas/yr**	G_{mag} * **mag**	**BP-RP * mag**	**VR * km/s**	ϵ_{VR} * **km/s**	VR_{exp} ** **km/s**	P_{tot} ***	**X pc**	**Y pc**	**Z pc**	**Flag ******
3217325130596656896	2.2437	−1.474	1.531	15.352	2.084	22.69	7.29	27.87	0.69	−383.3	−186.6	−129.7	B
3217341382752766592	2.4127	−1.968	0.674	15.958	2.244			27.89	0.78	−356.0	−172.7	−123.1	B
3216552169628139904	2.5268	−1.795	1.683	10.636	0.357	27.88	1.50	27.85	0.71	−339.5	−168.1	−114.1	B
3217691302328206080	2.3283	−1.602	1.039	13.726	1.196	24.69	7.18	27.90	0.65	−372.0	−175.3	−123.5	B
3217765618145551616	2.3669	−1.215	1.046	15.502	2.090			27.93	0.82	−367.3	−168.8	−122.6	B
3217765789944254720	2.3988	−0.912	1.155	15.880	2.160			27.93	0.62	−362.4	−166.6	−120.9	B
3217806506234469120	2.3512	−0.946	0.790	15.907	2.215			27.93	0.77	−370.8	−168.6	−122.1	B
3216104049917812608	2.3899	−1.979	1.380	15.187	1.836	34.96	9.73	27.85	0.84	−355.5	−179.7	−127.7	B

* Data from Gaia DR3; ** Expected radial velocities for supposed mean spatial motion of Group V (Section 4); *** Probability of membership in Group V; **** "G"—"Green" or "B"—"Blue" subset (see Section 4). Outliers in VR are marked with "O".

Notes

[1] http://stev.oapd.inaf.it/cmd (accessed on 6 February 2023)
[2] See note 1 above

References

1. Prusti, T. et al. [Gaia Collaboration]. The Gaia mission. *Astron. Astrophys.* **2016**, *595*, A1.
2. Brown, A.G.A. et al. [Gaia Collaboration]. Gaia Data Release 2. Summary of the contents and survey properties. *Astron. Astrophys.* **2018**, *616*, A1.
3. Castro-Ginard, A.; Jordi, C.; Luri, X.; Álvarez Cid-Fuentes, J.; Casamiquela, L.; Anders, F.; Cantat-Gaudin, T.; Monguió, M.; Balaguer-Núñez, L.; Solà, S.; et al. Hunting for open clusters in Gaia DR2: 582 new open clusters in the Galactic disc. *Astron. Astrophys.* **2020**, *635*, A45.
4. Castro-Ginard, A.; Jordi, C.; Luri, X.; Julbe, F.; Morvan, M.; Balaguer-Núñez, L.; Cantat-Gaudin, T. A new method for unveiling open clusters in Gaia. New nearby open clusters confirmed by DR2. *Astron. Astrophys.* **2018**, *618*, A59.
5. Castro-Ginard, A.; Jordi, C.; Luri, X.; Cantat-Gaudin, T.; Carrasco, J.M.; Casamiquela, L.; Anders, F.; Balaguer-Núñez, L.; Badia, R.M. Hunting for open clusters in Gaia EDR3: 628 new open clusters found with OCfinder. *Astron. Astrophys.* **2022**, *661*, A118.
6. Cantat-Gaudin, T.; Anders, F.; Castro-Ginard, A.; Jordi, C.; Romero-Gómez, M.; Soubiran, C.; Casamiquela, L.; Tarricq, Y.; Moitinho, A.; Vallenari, A.; et al. Painting a portrait of the Galactic disc with its stellar clusters. *Astron. Astrophys.* **2020**, *640*, A1.
7. Cantat-Gaudin, T.; Anders, F. Clusters and mirages: Cataloguing stellar aggregates in the Milky Way. *Astron. Astrophys.* **2020**, *633*, A99.
8. Kounkel, M.; Covey, K. Untangling the Galaxy. I. Local Structure and Star Formation History of the Milky Way. *Astron. J.* **2019**, *158*, 122.
9. Ratzenböck, S.; Meingast, S.; Alves, J.; Möller, T.; Bomze, I. Extended stellar systems in the solar neighborhood. IV. Meingast 1: The most massive stellar stream in the solar neighborhood. *Astron. Astrophys.* **2020**, *639*, A64.
10. Röser, S.; Schilbach, E. A census of the nearby Pisces-Eridanus stellar stream. Commonalities with and disparities from the Pleiades. *Astron. Astrophys.* **2020**, *638*, A9.
11. Meingast, S.; Alves, J.; Rottensteiner, A. Extended stellar systems in the solar neighborhood. V. Discovery of coronae of nearby star clusters. *Astron. Astrophys.* **2021**, *645*, A84.
12. Jerabkova, T.; Boffin, H.M.J.; Beccari, G.; de Marchi, G.; de Bruijne, J.H.J.; Prusti, T. The 800 pc long tidal tails of the Hyades star cluster. Possible discovery of candidate epicyclic overdensities from an open star cluster. *Astron. Astrophys.* **2021**, *647*, A137.
13. Brown, A.G.A. et al. [Gaia Collaboration]. Gaia Early Data Release 3. Summary of the contents and survey properties. *Astron. Astrophys.* **2021**, *649*, A1.
14. Vallenari, A. et al. [Gaia Collaboration]. Gaia Data Release 3. Summary of the content and survey properties. *Astron. Astrophys.* **2023**, *674*, A1. [CrossRef]
15. Vereshchagin, S.V.; Chupina, N.V. Star Structure of the Northern Part of the Orion Sword Region. *Astron. Rep.* **2023**, *67*, 336–392. [CrossRef]
16. Großschedl, J.E.; Alves, J.; Meingast, S.; Herbst-Kiss, G. 3D dynamics of the Orion cloud complex. Discovery of coherent radial gas motions at the 100-pc scale. *Astron. Astrophys.* **2021**, *647*, A91.
17. Alves, J.; Bouy, H. Orion revisited. I. The massive cluster in front of the Orion nebula cluster. *Astron. Astrophys.* **2012**, *547*, A97.
18. Caballero, J.A.; de Burgos, A.; Alonso-Floriano, F.J.; Cabrera-Lavers, A.; García-Álvarez, D.; Montes, D. Stars and brown dwarfs in the σ Orionis cluster. IV. IDS/INT and OSIRIS/GTC spectroscopy and Gaia DR2 astrometry. *Astron. Astrophys.* **2019**, *629*, A114.
19. Röser, S.; Schilbach, E.; Piskunov, A.E.; Kharchenko, N.V.; Scholz, R.D. A deep all-sky census of the Hyades. *Astron. Astrophys.* **2011**, *531*, A92.
20. Kharchenko, N.V.; Piskunov, A.E.; Schilbach, E.; Röser, S.; Scholz, R.D. Global survey of star clusters in the Milky Way. I. The pipeline and fundamental parameters in the second quadrant. *Astron. Astrophys.* **2012**, *543*, A156.
21. Spina, L.; Ting, Y.S.; De Silva, G.M.; Frankel, N.; Sharma, S.; Cantat-Gaudin, T.; Joyce, M.; Stello, D.; Karakas, A.I.; Asplund, M.B.; et al. The GALAH survey: Tracing the Galactic disc with open clusters. *Mon. Not. R. Astron. Soc.* **2021**, *503*, 3279–3296.
22. Bressan, A.; Marigo, P.; Girardi, L.; Salasnich, B.; Dal Cero, C.; Rubele, S.; Nanni, A. PARSEC: Stellar tracks and isochrones with the PAdova and TRieste Stellar Evolution Code. *Mon. Not. R. Astron. Soc.* **2012**, *427*, 127–145.
23. Sapozhnikov, S.; Kovaleva, D. Application of clustering algorithm to wide stellar pairs for unsupervised search of parts of disrupting clusters. *Open Astron.* **2021**, *30*, 191–202. [CrossRef]
24. Ester, M.; Kriegel, H.P.; Sander, J.; Xu, X. A Density-Based Algorithm for Discovering Clusters in Large Spatial Databases with Noise. In Proceedings of the Second International Conference on Knowledge Discovery and Data Mining, KDD'96, Portland, OR, USA, 2–4 August 1996; pp. 226–231.
25. Lindegren, L.; Klioner, S.A.; Hernández, J.; Bombrun, A.; Ramos-Lerate, M.; Steidelmüller, H.; Bastian, U.; Biermann, M.; de Torres, A.; Gerlach, E.; et al. Gaia Early Data Release 3. The astrometric solution. *Astron. Astrophys.* **2021**, *649*, A2.
26. Vereshchagin, S.V.; Tutukov, A.V.; Chupina, N.V. Scenario of OB-associations evolution. *INASAN Sci. Rep.* **2019**, *3*, 302–310. [CrossRef]

27. Getman, K.V.; Feigelson, E.D.; Kuhn, M.A.; Garmire, G.P. Gaia stellar kinematics in the head of the Orion A cloud: Runaway stellar groups and gravitational infall. *Mon. Not. R. Astron. Soc.* **2019**, *487*, 2977–3000.
28. Contreras Peña, C.; Naylor, T.; Morrell, S. Determining the recurrence time-scale of long-lasting YSO outbursts. *Mon. Not. R. Astron. Soc.* **2019**, *486*, 4590–4611.
29. Chumak, Y.O.; Rastorguev, A.S. Analysis of the structure and dynamics of the stellar tails of open star clusters. *Astron. Lett.* **2006**, *32*, 157–165. [CrossRef]
30. Jerabkova, T.; Boffin, H.M.J.; Beccari, G.; Anderson, R.I. A stellar relic filament in the Orion star-forming region. *Mon. Not. R. Astron. Soc.* **2019**, *489*, 4418–4428.
31. Bovy, J. galpy: A python Library for Galactic Dynamics. *Astrophys. J. Suppl. Ser.* **2015**, *216*, 29.
32. Vereshchagin, S.V.; Tutukov, A.V.; Chupina, N.V.; Postnikova, E.S.; Sizova, M.D. Binary Clusters: Theory and Observations. *Astron. Rep.* **2022**, *66*, 361–386. [CrossRef]
33. Taylor, M.B. TOPCAT & STIL: Starlink Table/VOTable Processing Software. In Proceedings of the Astronomical Data Analysis Software and Systems XIV, Pasadena, CA, USA, 24–27 October 2004; Shopbell, P., Britton, M., Ebert, R., Eds.; Astronomical Society of the Pacific Conference Series; Astronomical Society of the Pacific: San Francisco, CA, USA, 2005; Volume 347, p. 29.
34. Wenger, M.; Ochsenbein, F.; Egret, D.; Dubois, P.; Bonnarel, F.; Borde, S.; Genova, F.; Jasniewicz, G.; Laloë, S.; Lesteven, S.; et al. The SIMBAD astronomical database. The CDS reference database for astronomical objects. *Astron. Astrophys. Suppl. Ser.* **2000**, *143*, 9–22. [CrossRef]